Temperature- and pH-Dependent Morphology and FT−IR Analysis of Magnesium Carbonate Hydrates

Zhiping Zhang,[†] **Yajun Zheng,**[‡] **Yuwen Ni,**[†] **Zhongmin Liu,**[†] **Jiping Chen,***[,†] **and Xinmiao Liang**[†]

Dalian Institute of Chemical Physics, Chinese Academy of Sciences, 457 Zhongshan Road, Dalian 116023, China, and Institute of Chemistry for Functionalized Materials, Department of Chemistry, Liaoning Normal University, Dalian 116029, China

Various morphologies of magnesium carbonate hydrates have been synthesized by carefully adjusting the reaction temperature and pH value of the initial reaction solution in the precipitation process. At lower temperatures (from room temperature to 328 K) and lower pH values (variation with the reaction temperature), magnesium carbonate hydrates are prone to display needlelike morphology, and the axis diameter of the particles decreases with the increase of reaction temperature and pH value. With the further increase of the reaction temperature (333−368 K) and pH value, the sheetlike crystallites become the preferred morphology, and at higher temperatures and pH values, these crystallites tend to assemble into layerlike structures with diverse morphologies, such as spherical-like particles with rosette-like structure and cakelike particles built from sheetlike structure. Fourier transform infrared (FT−IR) spectra show that these various morphologies are closely related to their compositions. The needlelike magnesium carbonate hydrate has a formula of $MgCO_3 \cdot xH_2O$, in which the value x is greatly affected by the experimental conditions, whereas with the morphological transformation from needlelike to sheetlike structure, their corresponding compositions also change from $MgCO_3 \cdot xH_2O$ to $Mg_5(CO_3)_4(OH)_2 \cdot 4H_2O$ in the interval of 328−333 K.

1. Introduction

The design and fabrication of inorganic materials with well-controlled morphology have recently attracted a lot of interest because of their potentials in the design of new materials and devices, such as catalysis, medicine, electronics, ceramics, pigments, cosmetics,[1−4] etc. It is generally accepted that the particle shapes and their properties are closely related, and different forms of particles sometimes give different particle properties even for the same substance.[5] Therefore, it is crucial to fabricate materials with different morphologies according to the requirements of the devices, and the rules of controlled synthesis are important values for the practical application of materials.[6−10]

Magnesium carbonate hydrates are a class of materials of white odorless powder, including magnesite ($MgCO_3$), nesquehonite ($MgCO_3 \cdot 3H_2O$), hydromagnesite ($Mg_5(CO_3)_4(OH)_2 \cdot 4H_2O$), etc., which have been widely used because of their technological importance in various industrial applications (e.g., pharmaceuticals, cosmetic manufacturing, rubber industry, lithographing inks, and as precursors for other magnesium-based chemicals[11,12]). Up to now, a large number of chemical methods have been devoted to generating various morphologies of magnesium carbonate hydrates. For example, Mitsuhashi et al.[5] have developed a procedure to generate needlelike $MgCO_3 \cdot 3H_2O$ and microtube $Mg_5(CO_3)_4(OH)_2 \cdot 4H_2O$ by the carbonation of an aqueous suspension of magnesium hydroxide with carbon dioxide. Yan and Xue[13] have prepared nest-like $Mg_5(CO_3)_4$-

$(OH)_2 \cdot 4H_2O$ spheres by a self-assembly of nanosheets in the hydrothermal process, and they have also demonstrated that a pH variation of the initial reaction solution drastically affected the morphology of the obtained particles. Li et al.[14] have synthesized rosette-like $Mg_5(CO_3)_4(OH)_2 \cdot 4H_2O$ spheres by reacting anhydrous magnesium sulfate and urea via a hydrothermal method. Kloprogge et al.[15] have fabricated two different morphologies of $MgCO_3 \cdot 3H_2O$, a conglomerate consisted of very thin sheetlets and a well-formed needle, by adjusting the reaction conditions in the precipitation process, such as reaction temperature, stirring time, and aging time. The diversity of crystal morphologies that can be found for $MgCO_3 \cdot 3H_2O$ and $Mg_5(CO_3)_4(OH)_2 \cdot 4H_2O$ is a testimony to the fact that the macroscopic shape is highly sensitive to the growth conditions.[16] To our knowledge, no one has systematically investigated the change of morphology of $MgCO_3 \cdot 3H_2O$ or $Mg_5(CO_3)_4(OH)_2 \cdot 4H_2O$ with the variation of reaction conditions, such as reaction temperature, aging period, stirring time, and pH value, which to some extent, have improved our understanding of the mechanisms of their formation.

This study systemically investigated the influence of reaction temperature (from room temperature to 368 K) on the morphologies of $MgCO_3 \cdot 3H_2O$ and $Mg_5(OH)_2(CO_3)_2 \cdot 4H_2O$ in the precipitation process. As the transition between $MgCO_3 \cdot 3H_2O$ and $Mg_5(OH)_2(CO_3)_2 \cdot 4H_2O$ occurs in the interval of 328−338 K,[17−19] and the rate of change between them increases with the increase of temperature and pH value,[12] we further examined the effect of various pH values at 318 and 338 K on the morphologies of $MgCO_3 \cdot 3H_2O$ and $Mg_5(OH)_2(CO_3)_2 \cdot 4H_2O$, respectively. Additionally, because Fourier transform infrared spectroscopy (FT−IR) has been extensively used in the characterization of $MgCO_3 \cdot 3H_2O$ and $Mg_5(OH)_2(CO_3)_2 \cdot 4H_2O$,[15,20−26]

* Corresponding author. Phone: 86 411 84379562. E-mail: chenjp@dicp.ac.cn.
† Dalian Institute of Chemical Physics, Chinese Academy of Sciences.
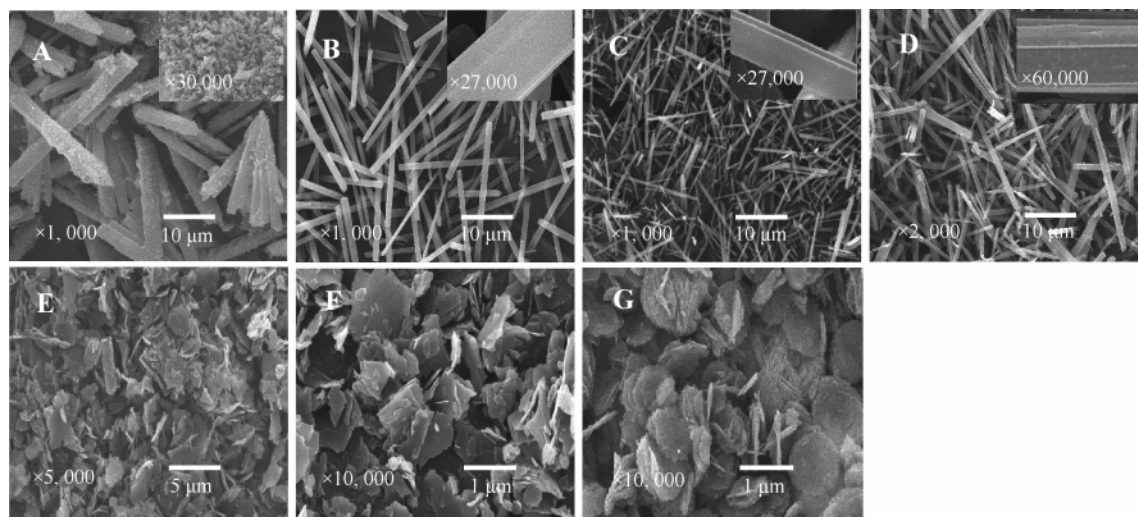‡ Institute of Chemistry for Functionalized Materials, Department of Chemistry, Liaoning Normal University.

Figure 1. Typical SEM morphologies for the particles from different temperatures (A, room temperature (291 K); B, 313 K; C, 323 K; D, 328 K; E, 333 K; F, 348 K; G, 368 K). Note: The inserted SEM morphologies in A−D are the corresponding magnification image of surface structure of an individual particle obtained from different temperatures.

which have provided valuable structure information for both compounds, the present paper also demonstrates the change patterns of the IR spectra for the particles obtained from various temperatures and pH values.

2. Experimental Section

2.1. Preparation. All chemical reagents, K_2CO_3, $Mg(NO_3)_2$, HNO_3, and KOH, used in the experiments were analytical grade without further purification. The detailed synthesis procedures are described as follows.

2.1.1. Procedures for Samples from Various Temperatures. The aqueous solutions of K_2CO_3 and $Mg(NO_3)_2$ were prepared by dissolving stoichiometric amount of K_2CO_3 and $Mg(NO_3)_2$ into 100 mL and 50 mL of distilled water, and their corresponding pH values were adjusted to 10.0 and 4.0 with dilute KOH and HNO_3 solution, respectively. The $Mg(NO_3)_2$ solution was then transferred to a 250 mL three-necked flask, and heated to a similar temperature as the water bath by keeping it to the desired range from 291 K (the room temperature) to 368 K. The K_2CO_3 solution was heated to the same temperature as the $Mg(NO_3)_2$ solution and rapidly added into the vigorously stirred (∼500 rpm) $Mg(NO_3)_2$ solution in 4−5 s. The mixture was further stirred for 4 min and then maintained at the temperature for 16 min. After that, a white precipitate was collected, filtered off, and washed with distilled water and ethanol several times. The obtained particles were dried in air at ca. 373 K for 4−5 h.

2.1.2. Procedures for Samples from Various pH Values. The major synthesis procedures for preparing the samples by the variation of pH value of the initial solution at 318 and 338 K were similar to those described above except the adjustment of the pH value. Before addition, the pH value of K_2CO_3 solution was adjusted in the range of 8.5−12.5 with dilute HNO_3 or KOH solution while keeping the pH value of $Mg(NO_3)_2$ solution equal to 4.0. In the following description, the pH value of K_2CO_3 solution was used as the pH value of the initial reaction solution.

2.2. Characterization. The morphology and particle size of as-synthesized particles were examined by scanning electron microscopy (SEM), and the images were taken with a JSM-6360LV scanning electron microscope. The IR spectra of the

obtained samples were recorded with a Perkin-Elmer GS-II FT−IR spectrometer in the range of 4000−400 cm^{-1}. The resolution was 4 cm^{-1} and eight scans were signal-averaged in each interferogram. The sample chamber was purged with N_2 before recording to minimize the effects caused by water vapor and carbon dioxide. Thermogravimetric analysis (TGA) was performed on a Perkin-Elmer SII Diamond TG-DTA instrument. The operating temperature was raised from 303 to 973 K with the rate of 10 K/min under N_2 atmosphere, and the used sample size varied between 3 and 5 mg.

3. Results and Discussion

3.1. Effect of the Reaction Temperature on Morphology. Figure 1 provides a set of typical SEM images corresponding to the samples from different reaction temperatures. As can be observed, these morphologies drastically change with the variation of the reaction temperature. When the reaction temperature increases from room temperature to 328 K, as shown in Figure 1A−D, the needlelike particles are produced, and the axis diameter varies with the increase of the reaction temperature. When the reaction is carried out at room temperature, the axis diameter is in the range of 3−6 μm. With the increase of the reaction temperature, the diameter gradually decreases, and it becomes 0.5−1.0 μm at 323 K. However, further increasing the temperature up to 328 K results in a slight increase of the axis diameter, and it becomes 0.8−1.5 μm. This case could be ascribed to the fact that at a lower reaction temperature (such as room temperature), the nuclei have a lower diffusion rate due to the viscous initial solution, which greatly limits their coalescence and self-assembly into needlelike particles. As a result, the growth rate of the nuclei is higher than the nucleation rate, and the particle grows into larger particles. With the increase of temperature, the viscosity of the initial solution gradually decreases, which accelerates the collision rate of the nuclei. A higher collision rate brings about a higher number of nucleated particles, so it is prone to produce smaller particles. When the temperature reaches 328 K, the higher collision rate may also contribute to an increase in the probability of coalescence, and the particle size has a slight increase.

After careful observation of these needlelike particles as shown in the magnification images of Figure 1A−D, it is clear
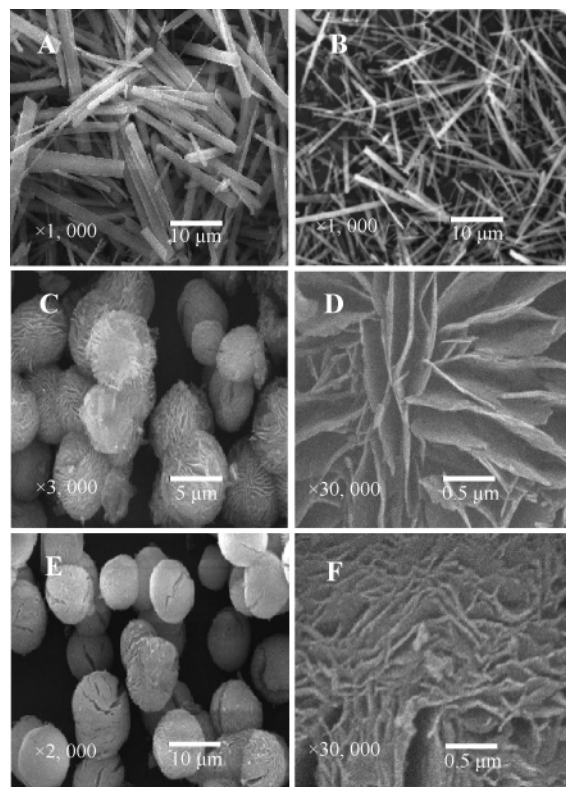
FT−IR Analysis of Magnesium Carbonate Hydrates

J. Phys. Chem. B, Vol. 110, No. 26, 2006 **12971**

Figure 2. Typical SEM morphologies for the particles from different pH values at 318 K (A, 8.5; B, 11.5; C and D, 12.0; E and F, 12.5). Note: D and F are the detailed wiew of surface structure of an individual particle in C and E, respectively.

Figure 3. Typical SEM morphologies for the particles from different pH values at 338 K (A, 8.5; B, 9.5; C, 10.5; D, 11.5; E and F, 12.5). Note: F is the magnification image of an individual particle in E from different angles.

that the surface structures of these particles also change with the increase of the reaction temperature. When the reaction is controlled at room temperature, the needlelike particles exhibit a cylindrical shape with coarse surface, which are composed of spherical-like crystallites with the diameter of 100−130 nm (Figure 1A). With the increase of the reaction temperature from 313 to 328 K, however, the needlelike particles display a smooth surface, and their corresponding surface structures also change from hexagonal prism to channeled shape as shown in the magnification images of Figure 1B−D. It is well-known that the morphologies of crystals are determined by the anisotropy of growth rates in different crystallographic directions.[27] Fast-growing crystallographic planes disappear and have little influence on the final crystal form. Slow-growing planes, however, dominate and determine the crystal form. The various surface structures in Figure 1A−D illustrate that the reaction temperature has a significant influence on the anisotropy of growth rates, so the particles display different macroscopic shapes with the variation of the reaction temperatures.

When the reaction temperature is up to 333−368 K, a great change on the morphologies of the particles takes place. As can be seen in Figure 1E−G, the morphology varies from sheetlike particles with a thickness of 20−30 nm to the layerlike particles with a thickness of 100−130 nm, which indicates that the latter might be gradually assembled from the former with the increase of reaction temperature.

3.2. Effect of pH Value of the Initial Reaction Solution on Morphology. The typical images of the particles synthesized at different pH values at 318 and 338 K are shown in Figures 2 and 3, respectively. At pH values below 9.5 for both temperatures, the particles all display a needlelike morphology, and the axis diameter of the particles decreases with the increase of the pH value, which is obvious in Figures 2A,B and 3A,B.
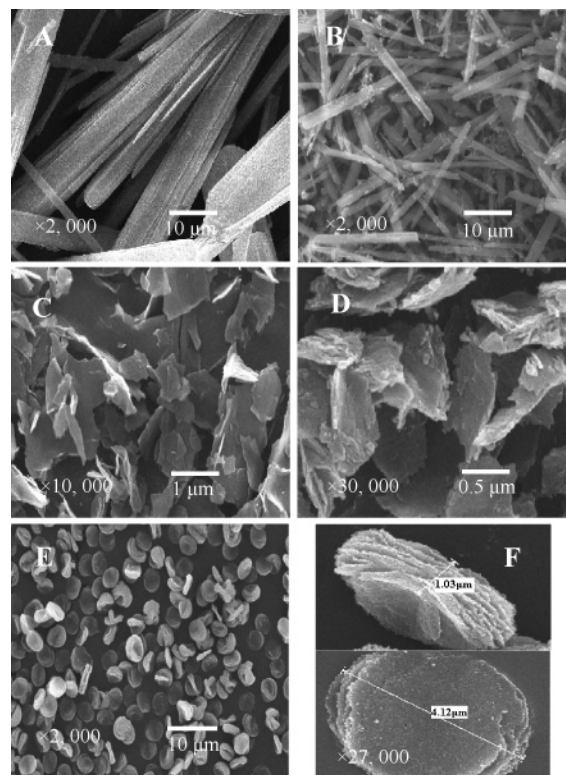
To our knowledge, it should be attributed to the fact that a lower pH value significantly restricts the nucleation rate of Mg^{2+} and CO_3^{2-} because many CO_3^{2-} ions exist in the form of HCO_3^-, so the nuclei are prone to assemble into larger particles. With the increase of the pH value, the nucleation rate gradually increases, and the nuclei tend to grow into smaller particles. From these images, it can be also noted that the needlelike morphology is still kept at 318 K and pH 11.5, whereas the highest pH value for this morphology at 338 K is 10.5, which can be ascribed, according to Botha and Strydom,[12] to the higher change rate from magnesium carbonate hydrate to basic magnesium carbonate at a higher temperature.

With the further increase of the pH value, the particles begin to display diverse morphologies. If the pH value is 12.0 at 318 K, the particles exhibit a spherical-like morphology (Figure 2C), and the average diameter is about 6.0 μm. From the detailed view of an individual spherical-like particle as shown in Figure 2D, it can be observed that these particles are built from a rosette-like structure with crystalline walls interconnected to each other. If the pH value is adjusted to 12.5, the particle is spherical in shape with a mean diameter of 10 μm (Figure 2E), which is composed of smaller nanosheets in a highly close-packed assembly (Figure 2F) relative to the particle obtained from pH 12.0. However, the particles at 338 K have distinct morphologies in contrast to those at 318 K. As can be observed, the sheetlike particles with irregular sizes (Figure 3C) are produced by adjusting the pH value to 10.5, whereas the layerlike particles composed of the sheetlike structures can be obtained when the pH value is increased to 11.5 (Figure 3D), which has a similar change pattern as the particles formed at different reaction temperature (Figure 1E−G). When the pH value is up to 12.5, it is interesting that the uniform cakelike particles built up by sheetlike structures are produced (Figure
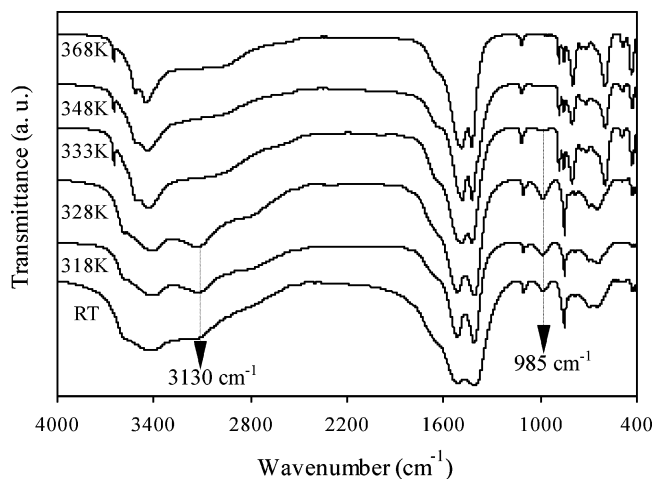
12972 *J. Phys. Chem. B, Vol. 110, No. 26, 2006*

Zhang et al.

Figure 4. FT−IR spectra of the particles from various temperatures. Note: RT denotes room temperature.

3E). From the magnification images shown in Figure 3F, it can be also observed that these particles display a longitudinal size of about 4.1 μm and thickness of about 1.0 μm. These results suggest that the formation of these cakelike particles may be via a process in which the sheetlike particles gradually assemble into layerlike structures, and the assembly speed is controlled by OH$^-$ in the solution. A higher concentration of OH$^-$ results in a more rapid assembly into microscopic particles, which agrees with the assembly mechanism reported by Yan and Xue.[13]

3.3. FT−IR Spectra Analysis. To better understand the morphology evolution with the variation of temperatures and pH values, the structure and compositional information of the particles have been recorded by the IR spectra.

Figure 4 shows the typical IR spectra of these particles obtained from different temperatures. It is obvious that the IR spectra vary significantly with the increase of the reaction temperature. For the particles obtained from the room temperature to 328 K, the IR spectra, as a whole, are very similar to those of $MgCO_3 \cdot 3H_2O$,[20,23] which are confirmed by the presence of 850 cm^{-1} (v_2 mode), 1105 cm^{-1} (v_1 mode), 1485 and 1420 cm^{-1} (v_3 mode) CO_3^{2-} adsorption bands. In addition, the O−H bending mode of water gives rise to a faint should band at 1645 cm^{-1}. These results indicate that the needlelike particles obtained below 328 K have a formula of $MgCO_3 \cdot xH_2O$. From this figure, however, it is interesting that there is a broad absorption band around 985 cm^{-1}, which is not always observed.[15,22,23] In the early literature, many authors regarded it as the characteristic absorption band of O−H$\cdots$O out-of-plane bending mode in bicarbonate ion,[20,25−26] suggesting that there are some bicarbonate ions in as-synthesized samples. At the same time, by comparison of these IR spectra with the report of White,[23] it can be seen that the broad bands in the range of 3600−3000 cm^{-1} have much difference between them, which may originate from a different number of water of crystallization. For confirming the composition of these particles, the TG analysis of the typical particles obtained from 318 K was performed, and its corresponding graph is given in the Supporting Information. After a calculation from the weight loss in different temperature stages of the TGA curve, the needlelike particles obtained from 318 K have a simple formula of $MgCO_3 \cdot 1.3H_2O$, whereas in many previous reports[15,17−20] the particles obtained below 328 K should have a formula of $MgCO_3 \cdot 3H_2O$. The difference between them can be attributed, according to our recent study (unpublished results), to the different preparation conditions.

With the increase of the reaction temperature up to 333 K, the IR spectra take place a great change. In contrast to the IR spectra of the particles obtained below 328 K, a sharp band around 3650 cm^{-1} corresponding to the free O−H vibration appears, and the bands between 3600 and 3400 cm^{-1} also become narrower. In addition, the carbonate bending vibrations split into three absorption bands at ~800 (the strongest), 850, and 880 cm^{-1}. All of the above features were suggested as the characteristic adsorption of $Mg_5(CO_3)_4(OH)_2 \cdot 4H_2O$,[12,22] which is consistent with the TG analysis of the typical particles from 348 K (see Supporting Information). The transition interval found in the present study is in good agreement with the results described in the literature,[17−19] which reported that the transition between $MgCO_3 \cdot 3H_2O$ and $Mg_5(OH)_2(CO_3)_2 \cdot 4H_2O$ occurred in the interval of 328−338 K.

For the particles from various pH values at 318 and 338 K, as shown in Figure 5A and B, the IR spectra have a similar change pattern as those of the particles from different temperatures as shown in Figure 4. At pH values below 9.5, the IR spectra of the particles from 318 and 338 K can be assigned to $MgCO_3 \cdot xH_2O$, and with the increase of the pH value it gradually transforms into $Mg_5(CO_3)_4(OH)_2 \cdot 4H_2O$. These results indicate that at lower temperatures and pH values the particles are all prone to produce needlelike $MgCO_3 \cdot xH_2O$, and in contrary Mg_5-$(CO_3)_4(OH)_2 \cdot 4H_2O$ is preferred at higher temperatures and pH values.

At the same time, it can be noted that for the particles at 318 K, the pH value of the transformation between $MgCO_3 \cdot xH_2O$ and $Mg_5(CO_3)_4(OH)_2 \cdot 4H_2O$ is 11.5−12.5, whereas the value at 338 K decreases to 9.5−10.5, which demonstrates that the rate of change between them increases with the increase of temperature.[12] In addition, for the particles from 8.5 to 9.5 at 318 K the broad band around 985 cm^{-1} becomes much weaker relative to that at 338 K, and it almost disappears when the pH value is up to 10.5. With the disappearance of the band at 985 cm^{-1}, however, an extra band at 2344 cm^{-1} begins to appear, and its intensity also gradually increases. In the study of magnesium carbonate hydrates, Botha and Strydom[12] also observed this band, and they regarded this band as either a CO_2 inclusion or a terminal CO_2 in the rehydration particles because it corresponds to the position of the v_3 fundamental of CO_2.[28] As discussed above, the band at 985 cm^{-1} can be attributed to the characteristic absorption band of bicarbonate ion, which illustrates that the band at 2344 cm^{-1} may be the characteristic absorption band of CO_2 resulting from the decomposition of bicarbonate ion in these particles. This assumption can be further confirmed by the IR spectra of other particles after calcination at different temperatures (see Supporting Information).

A comparison of Figure 5A(a−d) with Figure 5B(a−b), it can be found that for the particles from pH 8.5−9.5 at 338 K, there is a broad band at ~3130 cm^{-1} resulting from the O−H vibration, whereas for the particles from pH 8.5−11.5 at 318 K this band becomes very weak. The difference between them may come from different number of water of crystallization, which is confirmed by the results of TG analyses (see Supporting Information). After a calculation from the data of TG analysis, the typical particles from pH 11.5 at 318 K (Figure 5A(d)) have a simple formula of $MgCO_3 \cdot 0.3H_2O$, whereas the particles from pH 8.5 at 338 K (Figure 5B(a)) have a formula of $MgCO_3 \cdot 0.8H_2O$, which displays that the variation of experimental conditions has a significant effect on the value x in $MgCO_3 \cdot xH_2O$.

FT−IR Analysis of Magnesium Carbonate Hydrates

J. Phys. Chem. B, Vol. 110, No. 26, 2006 **12973**
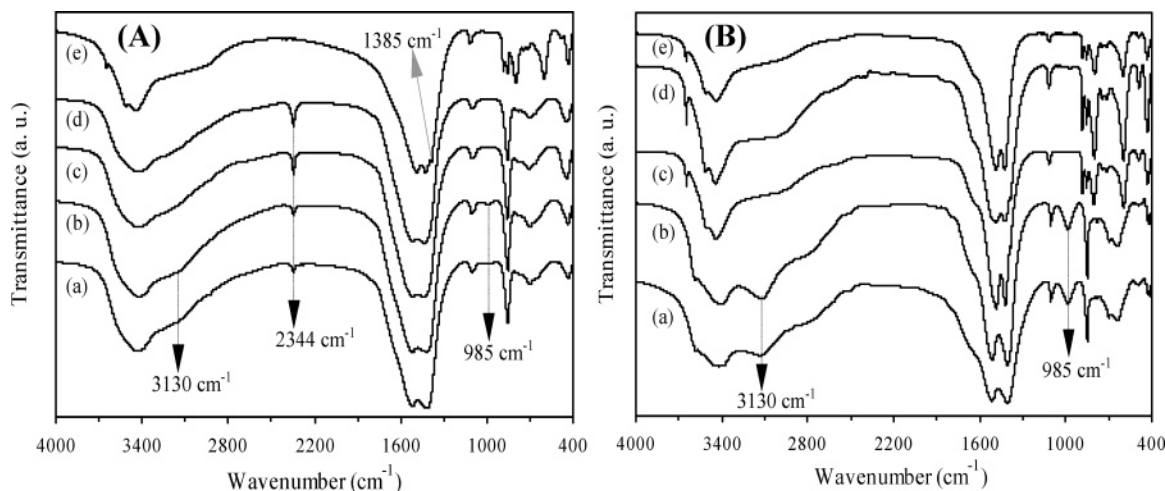

Figure 5. FT−IR spectra of the particles from different pH values at 318 K (A)-(a, 8.5; b, 9.5; c, 10.5; d, 11.5, and e, 12.5) and 338 K (B)-(a, 8.5; b, 9.5; c, 10.5; d, 11.5, and e, 12.5). Note: the band at 1385 cm^{-1} can be assigned to the characteristic absorption band of NO$_3^-$ remaining in the sample.

4. Conclusions

The synthesis and vibrational spectra of various morphologies of magnesium carbonate hydrates prepared at different reaction temperatures and pH values were studied by SEM, FT−IR, and TG analyses. Based on the results discussed in this paper, it can be concluded that (i) at reaction temperatures below 328 K and lower pH values, the nuclei are all prone to assemble into needlelike morphology, which has a formula of MgCO$_3$·xH$_2$O (the x value varies with the reaction conditions), and the size of the needlelike particle can be adjusted by the reaction temperature and pH value of the initial reaction solution, (ii) there are a certain amount of bicarbonate ions in the MgCO$_3$·xH$_2$O, which can be confirmed by the characteristic absorption bands of 2344 and 985 cm^{-1}, and (iii) at reaction temperatures above 333 K and higher pH values, the sheetlike structure is the preferred morphology, and it has a formula of Mg$_5$(CO$_3$)$_4$-(OH)$_2$·4H$_2$O; with the further increase of reaction temperature and pH value, the sheetlike structure will transfer into different layerlike particles, such as spherical-like and cakelike particles. The investigation of the conversion between various morphologies with the variation of temperature and pH value described here may be applicable to explain the formation of magnesium carbonate hydrates of other shapes, and it also serves a promising basis for systemically studying magnesium carbonate hydrates.

Supporting Information Available: The TG and DTG graphs of the particles from 318 and 348 K, the variety of IR spectra with the change of calcination temperature, and the TG and DTG graphs of the particles from pH 11.5 at 318 K and from pH 8.5 from 338 K. This material is available free of charge via the Internet at http://pubs.acs.org.

References and Notes

(1) Shi, H. T.; Qi, L. M.; Ma, J. M.; Cheng, H. M. *J. Am. Chem. Soc.* **2003**, *125*, 3450.

(2) Peng, Q.; Dong, Y. J.; Li, Y. D. *Angew. Chem., Int. Ed.* **2003**, *42*, 3027.

(3) Sun, S.; Murray, C. B.; Weller, D.; Folks, L.; Moser, A. *Science* **2000**, *287*, 1989.

(4) Bruchez, M.; Moronne, M.; Gin, P.; Weiss, S.; Alivisatos, A. P. *Science* **1998**, *281*, 2013.

(5) Mitsuhashi, K.; Tagami, N.; Tanabe, K.; Ohkubo, T.; Sakai, H.; Koishi, M.; Abe, M. *Langmuir* **2005,** *21*, 3659.

(6) Hu, X. L.; Zhu, Y. J. *Langmuir* **2004**, *20*, 1521.

(7) Rautaray, D.; Ahmad, A.; Sastry, M. *J. Am. Chem. Soc.* **2003**, *125*, 14656.

(8) Tian, Z. R.; Voigt, J. A.; Liu, J.; Mckenzie, B.; Mcdermott, M. J. *J. Am. Chem. Soc.* **2002**, *124*, 12954.

(9) Rautaray, D.; Sinha, K.; Shankar, S. S.; Adyanthaya, S. D.; Sastry M. *Chem. Mater.* **2004**, *16*, 1356.

(10) Liao, H. W.; Wang, Y. F.; Lihnju, X. M.; Li, Y. D.; Qian, Y. T. *Chem. Mater.* **2000**, *12*, 2819.

(11) Freitag, F.; Kleinebudde, P. *Euro. J. Pharm. Sci.* **2003**, *19*, 281.

(12) Botha, A.; Strydom, C. A. *Hydrometallurgy* **2001**, *62*, 175.

(13) Yan, C. L.; Xue, D. F. *J. Phy. Chem. B* **2005**, *109*, 12358.

(14) Li, Q.; Ding, Y.; Yu, G. H.; Li, C.; Li, F. Q.; Qian, Y. T.; *Solid State Commun.* **2003**, *125*, 117.

(15) Kloprogge, J. T.; Martens, W. N.; Nothdurft, L.; Duong, L. V.; Webb, G. E. *J. Mater. Sci. Lett.* **2003**, *22*, 825.

(16) Davey, R. J.; Whiting, M. J. L. *J. Cryst. Growth* **1982**, *58*, 304.

(17) Davies, P. J.; Bubela, R. *Chem. Geol.* **1973**, *12*, 289.

(18) Yanat'yeva, O. K. *Doklady Atad. Nauk, S.S.S.R.* **1954**, *96*, 777.

(19) Rassonskaya, L. S. *Russian J. Inorg. Chem.* **1961**, *6*, 730.

(20) Farmer, V. C. *The Infrared Spectra of Minerals;* Mineralogical Society: London, 1974.

(21) Coleyshaw, E. E.; Crump, G.; Griffith, W. P. *Spectrochim. Acta A* **2003**, *59*, 2231.

(22) Lanas, J.; Alvarez, J. I. *Thermochim. Acta* **2004**, *421*, 123.

(23) White, W. B. *Am. Mineral.* **1971**, *56*, 46.

(24) Kelleher, I. J.; Redfern, S. A. T. *Mol. Simulat.* **2002**, *28*, 557.

(25) Miller, F. A.; Wilkins, C. H. *Anal. Chem.* **1952**, *24*, 1253.

(26) Nakamoto, K.; Sarma, Y. A.; Ogoshi, H. *J. Chem. Phy.* **1965**, *43*, 1177.

(27) Liang, J.; Ma, Y.; Zheng, Y.; Davis H. T. *Langmuir* **2001**, *17*, 6447.

(28) Schrader, B. *Infrared and Raman spectroscopy: methods and applications;* Wiley: London, 1989.